Published in final edited form as:

J Immunol. 2019 January 01; 202(1): 194–206. doi:10.4049/jimmunol.1800777.

The GTPase Rab1 is required for NLRP3 inflammasome activationand inflammatory lung injury

Yuehui Zhang[*,#,1], **Lijun Wang**[#,1], **Yang Lv**[*], **Chunling Jiang**[*], **Guangyu Wu**[‡], **Randal O. Dull**[*], **Richard D. Minshall**[*,†], **Asrar B. Malik**[†], and **Guochang Hu**[*,†,§]

[*]Department of Anesthesiology, University of Illinois College of Medicine, Chicago, IL 60612;

[†]Department of Pharmacology, University of Illinois College of Medicine, Chicago, IL 60612;

[#]Department of Critical Care Medicine, Affiliated Baoan Hospital of Shenzhen, Southern Medical University, Shenzhen, Guangdong 518101, China

[‡]Department of Pharmacology and Toxicology, Medical College of Georgia, Augusta University, Augusta, GA 30912

[§]Department of Anesthesiology, The Affiliated Hospital of Xuzhou Medical University, Xuzhou, Jiangsu, China 221008.

Abstract

Uncontrolled inflammatory response during sepsis predominantly contributes to the development of multi-organ failure and lethality. However, the cellular and molecular mechanisms for excessive production and release of proinflammatory cytokines are not clearly defined. Here, we show the crucial role of the GTPase Ras-related protein in brain (Rab)1a in regulating the NLRP3 inflammasome activation and lung inflammatory injury. Expression of dominant negative Rab1 N124I plasmid in bone marrow-derived macrophages prevented the release of IL-1β and IL-18, NLRP3 inflammasome activation, production of pro-IL-1β and pro-IL-18, and attenuated Toll-like receptor 4 surface expression and nuclear factor-κB activation induced by bacterial lipopolysaccharide and ATP compared with control cells. In alveolar macrophage-depleted mice challenged with cecal ligation and puncture, pulmonary transplantation of Rab1a-inactivated macrophages by expression of Rab1 N124I plasmid dramatically reduced the release of IL-1β and IL-18, neutrophil count in bronchoalveolar lavage fluid, and inflammatory lung injury. Rab1a activity was elevated in alveolar macrophages from septic patients and positively associated with severity of sepsis and respiratory dysfunction. Thus, inhibition of Rab1a activity in macrophages resulting in the suppression of NLRP3 inflammasome activation may be a promising target for the treatment of patients with sepsis.

Correspondence should be addressed to:Guochang Hu, M.D., Ph.D., 3200W UICH, MC 515, Department of Anesthesiology, University of Illinois College of Medicine, 1740 W. Taylor St. Chicago, IL 60612-7239, USA, Phone: (312) 996-4692, Fax: (312) 996-1225, gchu@uic.edu.

[1]These authors equally contribute to this manuscript.

Disclosure

The authors have no financial conflict of interest.

Introduction

The host immune response to bacterial infection is an important determinant of the pathogenesis and outcome of sepsis. Upon antigen recognition, immune cells are activated and release pro-inflammatory cytokines that drive the “cytokine storm” and uncontrolled inflammatory response and lead to serious multi-system dysfunction and death (1). Among pro-inflammatory cytokines, IL-1β is a key proinflammatory cytokine released at sites of infection or injury, that stimulates secretion of numerous downstream pro-inflammatory mediators such as TNF-α, IL-1, IL-6, and cyclooxygenase type-2 (2). Furthermore, IL-1β has been demonstrated to be the most biologically active cytokines in the lungs of patients with acute lung injury (3). However, the cellular and molecular mechanism by which the active IL-1β is released from cells remains elusive.

The nucleotide binding domain-like receptor family, pyrin domain containing 3 (NLRP3) inflammasome consists of three molecules: cytosolic innate immune sensor NLRP3, adaptor apoptosis-associated speck-like protein containing a caspase recruitment domain (ASC), and caspase-1. Activation of NLRP3 inflammasome requires two signals: a priming signal is usually induced by TLR-mediated NF-κB signaling which triggers production of pro-IL-1β and pro-IL-18; and a second NLRP3-specific signal is activated by a diverse array of stimuli such as reactive oxygen species (ROS), extracellular ATP, alum, and pore-forming toxin nigericin (4–6). Upon activation, ASC associates with NLRP3 and pro-caspase-1 through homotypic domain interaction to form the functional inflammasome. A conformational change in pro-caspase-1 due to its recruitment to the inflammasome induces its autocatalytic activity, resulting in self-cleavage to release proteolytically active caspase-1, which cleaves pro-IL-1β and pro-IL-18 to mature IL-1β and IL-18 forms (7). Although the regulatory mechanism of NLRP3 activation is not completely known, NLRP3 deficient mice have been recently reported to be resistant to polymicrobial sepsis-induced lethality (8).

Rab (Ras-related proteins in brain) GTPases are localized at distinct membrane-bound compartments and mediate virtually all stages of membrane trafficking from the vesicle budding at the donor membrane, transport, tethering, and docking to vesicle fusion at the target membrane (9, 10). Amongst Rab GTPases, Rab1, the mammalian homologue of yeast protein transport 1 (Ypt1), is a central regulator of dynamic membrane trafficking between endoplasmic reticulum (ER) and Golgi apparatus in the secretory pathway. Beyond their classical vesicular transport functions, Rab1 proteins also regulate expression of cell-surface receptors, cell migration, and nutrient sensing (11). There are two Rab1 isoforms, Rab1a and Rab1b, which share 92% amino-acid sequence homology with most differences in the carboxyl terminus (12). Rab1a and Rab1b are mainly expressed at the ER and the Golgi membrane, and are also detected in lipid rafts (13) and autophagosomes (14). In the present study, we identified Rab1a as a crucial regulator for the release of proinflammatory cytokines IL-1β and IL-18 in macrophages and lung inflammatory injury.

Materials and Methods

Mice

C57BL/6J mice were acquired from Jackson Laboratory (Bar Harbor, ME), housed in a specific pathogen–free barrier facility, and used in experiments at 12–16 weeks of age. All animal protocols were approved by the Institutional Animal Care and Use Committee of the University of Illinois at Chicago. All studies were performed under anesthesia using either 1–3% isoflurane (inhalation) or ketamine/xylazine (100 mg/kg/12.5 mg/kg, i.p.).

Patients

Ten patients meeting the Sepsis-3 clinical criteria (15) and ARDS (16) were enrolled into the current study within the first 24 h after they were admitted to the intensive care unit (ICU) of the Affiliated Baoan Hospital of Nanfang Medical University between August 2017 and December 2017. Patients were included if they had suspected or confirmed infection, an increase in the Sequential (Sepsis-related) Organ Failure Assessment (SOFA) score of two or more points for organ dysfunction, and arterial oxygen partial pressure (PaO_2)/ fraction of inspired oxygen (FiO_2) ≤ 300 mm Hg with positive end-expiratory pressure (PEEP) ≥5 cm H_2O. Exclusion criteria included age <18 years, pregnancy, human immunodeficiency virus infection, treatment with corticosteroids or immunosuppressants, and unwilling to consent to the interventions. Ten non-septic critically ill patients with no evidence of bacterial or fungal infection were recruited as controls. Bronchoalveolar lavage fluid (BALF) samples were obtained 6–12 h after admission. Acute Physiology and Chronic Health Evaluation (APACHE) II scores and PaO_2/FiO_2 were calculated for each patient. The patients' clinical and demographic data, including age, sex, APACHE II scores PaO_2/FiO_2 as well as the levels of IL-1β and IL-18 in BALF were recorded (Table 1). The study protocol (BYL20170615) was approved by institutional review board, and written informed consent obtained from legal next of kin.

Isolation of alveolar macrophages from patients

Alveolar macrophages were isolated from BALF obtained from patients via fiber-optic bronchoscopy as described previously (17). Briefly, a fiber-optic bronchoscope was inserted into the tracheobronchial tree. The lung was lavaged with 30 ml aliquots of warmed sterile saline to a total volume of 180 ml. The retrieved BALF was filtered and then centrifuged at 300 g, 4°C for 10 min. Alveolar macrophages were isolated by plating total cells in tissue culture dishes for 2 h at 37°C and removing non-adherent cells. The purity of alveolar macrophages was more than 95%, confirmed by flow cytometric analysis of CD68 expression.

Isolation and culture of murine bone marrow-derived macrophages

Murine bone marrow-derived macrophages (BMDMs) were isolated and cultured as described previously (18). Bone marrow was flushed out of tibias and femur with differentiation medium (RPMI 1640 medium supplemented with 12.5% FBS, 20% L929-cell conditioned medium, 10 mM L-glutamine, 100 IU/ml penicillin, and 100 mg/ml streptomycin). Cells (4×10^5) were plated in 10 ml macrophage complete medium and

incubated at 37°C and 5% CO_2. On d 3, 5 ml macrophage complete medium was added to each dish. After 7 d in culture, non-adherent cells were >95% pure macrophages, as determined by the expression of cell-surface markers HLA-DR, CD11b, and CD206.

RNA interference and cDNA transfection

BMDMs were transfected with small interfering (si) RNA using Lipofectamine® RNAiMAX Reagent (Invitrogen). BMDMs (6.3×10^5) were grown in 6-well plates with antibiotic-free RPMI 1640 medium supplemented with 10% FBS and incubated at 37° C in a CO_2 incubator for 24 h. Cells were then transfected with 5–20 nM Rab1a siRNA or non-targeting control siRNA (Dharmacon) according to the protocol provided by the manufacturer. Transfection of cDNA into BMDMs was performed using a 4D Nucleofector X-Unit (Lonza) according to the manufacturer's instructions. Briefly, cells were pre-incubated in RPMI 1640 medium containing 20% FBS at 37°C, centrifuged at 200 g for 10 min, and then resuspended in P2 Nucleofector Solution (Lonza) to a concentration of 2×10^6 cells/100 μl (containing 2 μg plasmid cDNA). Nucleofection was performed using program CM189.

Cytotoxicity detection

Cytotoxicity was assessed by determining the total lactate dehydrogenase (LDH) released in the medium upon cell lysis, using Cytotoxicity Detection Kit (LDH). LDH release was expressed as a percentage of LDH in medium to total LDH.

Western blotting and immunoprecipitation

Western blotting was performed with samples from the cultured medium and the cell lysates (19). The cell culture media were collected and concentrated using Amicon® Ultra 10K Filter Devices (Millipore). The cells were lysed with radioimmunoprecipitation assay (RIPA) buffer (Boston Bio Products, BP-115). Samples were electrophoresed on 8–14% SDS-PAGE and then transferred to Immobilon-P PVDF transfer membranes (Merck Millipore). The membrane was blocked, probed with primary Abs overnight at 4°C, and then incubated with HRP-conjugated secondary Abs (1:3000~5000) at room temperature for 1 h. The protein bands were detected with Odyssey Fc Imager (LI-COR Biosciences). Relative band densities of proteins were quantified using ImageJ Software (NIH).

Immunoprecipitation was performed as described previously (19). BMDMs were lysed in immunoprecipitation lysis buffer (1% NP-40, 50 mM Tris-HCl, pH 7.4, and 150 mM NaCl) supplemented with 1 mM PMSF and protease inhibitor. The cell lysates were incubated with an appropriate Ab overnight at 4°C, followed by addition of 20 μl protein A/G PLUS-agarose beads for 2 h at 4°C. The resulting immunoprecipitates were dissolved in SDS-PAGE sample buffer for electrophoresis and immunoblot analysis

Rab1a activation assay

Cells were lysed with ice cold lysis buffer (50 mM Tris-HCl, pH 7.5, 2% Nonidet P-40, 10 mM $MgCl_2$, 300 mM NaCl, and protease inhibitor). Collected lysates were incubated with anti-Rab1-GTP monoclonal Ab and Protein A/G PLUS-agarose beads at 4°C for 1 h. The

beads were collected by centrifugation of lysates for 1 min at 5000 g. Samples were finally dissolved in SDS buffer for Western blotting.

Flow cytometry

BMDMs were detached with 10 mM EDTA/PBS solution. The pellets were collected by centrifugation at 200 g for 5 min and washed with cold staining buffer (PBS without Ca^{2+} and Mg^{2+} containing 0.5% BSA). BMDMs were resuspended in staining buffer at a final cell concentration of 1×10^6/50 μl, incubated with 0.5 μg of purified anti-mouse CD16/CD32 Ab for blocking non-specific Fc-mediated interactions and then with anti-mouse CD284 (TLR4) PE (0.01 μg/μl) Ab or mouse IgG2a κ isotype control Ab for 45 min on ice, and analyzed by flow cytometry (Becton Dickinson LSR I).

Mitochondria-associated ROS levels were measured in BMDMs by staining cells with MitoSOX (20, 21). Briefly, cells were incubated for 30 min at 37°C in a 10 μM MitoSOX™ Red (Invitrogen-Molecular Probes) solution prepared in 4:1 (v/v) DMEM/PBS. Cells were harvested with 500 μl of trypsin-EDTA solution, centrifuged at 2300 g for 5 min, and resuspended in 3 ml of 2% (v/v) FBS/PBS. Stained cells were determined with a Beckman Gallios and data analyzed with FlowJo10 analytical software (TreeStar). The mean fluorescence of the cell samples was then normalized to the unstained group.

Cell surface biotinylation and endocytosis assay

Biotinylation of cell surface proteins was performed as described as previously (22). BMDMs were incubated with 1.5 mg/ml sulfosuccinimidyl,2-(biotinamido) ethyl-dithioproprionate (sulfo-NHS-SS-biotin) (Pierce) for 30 min at 4°C with gentle shaking. Sulfo-NHS-SS-biotin blocking reagent (50 mM NH_4Cl in PBS containing 1 mM $MgCl_2$ and 0.1 mM $CaCl_2$) was added to quench any unreacted biotin reagent. The biotinylated cells were incubated with LPS (20 ng/ml) at 37°C for 20 min to allow protein endocytose and then incubated with sodium 2-mercaptoethanesulfonate (MESNA, 100 mM) to remove any residual surface biotin. Following cell lysis, biotinylated proteins were isolated by incubation with NeutrAvidin beads and detected by immunoblotting. The internalization rate was expressed as the ratio of the amount of internalized protein to the total surface control labeled at time 0 min.

Immunofluorescence

Immunofluorescence was performed as described previously (23). Briefly, cells plated on coverslips were fixed with 4% paraformaldehyde for 10 min, permeabilized with 0.3% Triton X-100 in PBS for 5 min, and then incubated with primary Abs at 4°C overnight, followed by incubation with fluorescent secondary Abs (1:750) for 1 h. The cells were mounted on glass slides using antifade mounting medium with DAPI (Vectorshield, Molecular Probes). Images were captured by a Zeiss LSM 880 laser-scanning confocal microscope equipped with Argon laser for 488 nm, Diode 405–30 for 405nm, Diode pumped solid state laser (DPSS) 561–10 for 561 nm and HeNe633 laser for 633 nm excitation and beam splitters MBS 488/561/633 and MBS-405.

ASC oligomerization assay

ASC oligomerization was detected as described previously (24). Cells were lysed in lysis buffer A (20 mM HEPES, 10 mM KCl, 1.5 mM $MgCl_2$, 1 mM EDTA, and protease inhibitor), harvested, and sheared by passing them through a 27–1/2G needle for 20 times. The lysates were centrifuged at 340 g for 8 min to remove the intact cells and nuclei. The supernatants were collected, mixed with CHAPS buffer (20 mM HEPES, 5 mM $MgCl_2$, 0.5 mM EDTA, 0.1% CHAPS, and protease inhibitor) and centrifuged at 2650 g for 8 min. The pellets were resuspended in CHAPS buffer containing chemical cross-linked reagent (2 mM disuccinimidyl suberate), rotated at 4°C for 2 h. The reaction was quenched by adding a final concentration of 20 mM Tris (pH 7.5). Pellets containing the ASC were collected by centrifugation at 3300 g for 10 min and dissolved in SDS buffer for Western blotting.

Preparation of mitochondria and cytochrome C oxidase activity assay

Mitochondria were prepared as described previously (25). BMDMs were washed, resuspended in Mg Resuspension Buffer (MgRSB) (10 mM NaCl, 1.5 mM $MgCl_2$, 10 mM Tris-HCl, pH 7.5), incubated at 4°C for 10 min, and homogenized. The homogenate was diluted with 1.3 volumes of mannitol-sucrose buffer (MSB) (0.525 M mannitol, 175 mM sucrose, 12.5 mM EDTA, 12.5 mM Tris-HCl, pH 7.5) and centrifuged at 1000 g for 10 min to remove nuclei, unbroken cells, and large membrane fragments. The supernatant was transferred to a clean centrifuge tube and centrifuged at 16,000 g for 30 min. The pellets (mitochondrial fraction) were collected and digested with DNase I (Sigma) at 37°C for 30 min.

Cytochrome C oxidase (CcO, or complex IV) activity was measured spectrophotometrically using Complex IV Rodent Enzyme Activity Microplate Assay Kit following the manufacturer's instructions (26). In brief, BMDMs were lysed with the extraction detergent (1:10 volume detergent) followed by centrifugation at 13,000 g for 40 min at 4°C. The supernatants were collected, loaded on the plate with a positive control sample and buffer control included as null reference, and incubated at room temperature for 3 h. Each well was rinsed twice with solution 1 and then 200 μl of assay solution was added. CcO activity was determined by measuring absorbance at 550 nm at 30°C for 2 h, with approximately 2-min intervals. The results were expressed as a percentage of CcO activity of the control (Vector) BMDMs stimulated with LPS+ATP.

Cytokine measurements

The concentrations of IL-1β and IL-18 in the medium and BALF were measured with ELISA kits (BioLegend) or Cytometric Bead Array (CBA) kits (eBioscience) according to the manufacturers' instructions.

Mouse models

Mice were depleted of alveolar macrophages by i.t. instillation of clodronate liposome (100 μl, 1:2 dilution in PBS) to anesthetized (ketamine 100 mg/kg, i.p.) mice (27). PBS or BMDMs transfected with a vector, Rab1a WT, or Rab1a N124I cDNA (2×10^6 cells, 200 μl of total volume each) were given to alveolar macrophage–depleted mice via i.t. instillation.

Polymicrobial sepsis in mice was induced by cecal ligation and puncture (CLP) as described previously (28). Briefly, approximately two-thirds of the cecum was ligated and a single puncture into the ligated portion made with a 16-gauge needle. The cecum was gently squeezed to extrude a small amount of cecal content from the perforation sites and then returned to the peritoneal cavity. Mice were resuscitated with intraperitoneal injection of 1 ml normal saline pre-warmed to 37°C. Sham-operated mice underwent the same procedure except for ligation and puncture of the cecum. Following the operation, all mice received 0.2 ml of bupivacaine hydrochloride (0.25%) at the end of the operation.

Determination of polymorphonuclear neutrophil (PMN) counts in BALF

Mice were anesthetized with ketamine/xylazine (100 mg/kg/12.5 mg/kg, i.p.) mixture. BAL was performed by intratracheal injection of 1 ml PBS and repeated three times. BALF was collected, centrifuged at 500 g for 5 min at 4°C. After total cell counts were manually obtained with a hemocytometer, the concentration of cells was adjusted to 1×10^5 cells/ml. Then 200 μl cells were cytospun onto slides at 300 g for 5 min with a cytocentrifuge (Shandon). Slides were immediately fixed, stained using Diff-Quick dye (Siemens, B4132–1A), and examined by microscopy. The percentage of PMNs was calculated after counting 300 cells in randomly selected fields.

Measurement of myeloperoxidase (MPO) activity

Lung MPO activity as a marker of PMN infiltration was determined following the manufacturer's protocol (29). MPO activity was assessed in 100 μl of supernatants in duplicate by using development reagent at 450 nm and expressed as change in absorbance per milligram of protein.

Determination of inflammatory lung injury

Total protein concentration in BALF was measured using Bradford protein assay (Bio-Rad). The results were converted to μg/μl using values based on a standard curve generated with serial dilutions of BSA.

Evans blue-albumin (30 mg/kg) was injected to the caudal vein of mice 35 min before lung collection. The tissues were homogenized and incubated with 1 ml formamide for 18 h at 60°C followed by centrifuged at 13,000 g for 20 min. The absorbance of lung supernatants was determined at 620 nm and corrected for the presence of heme pigments as follows: A620 (corrected) = A620 - (1.1649 × A740 + 0.004) (30). The Evans blue index was calculated as the amount of dye in the lung to the weight of lung tissue.

Lung histology and lung injury scoring

The lung tissue was perfused and fixed with 10% buffered formalin. Formalin-fixed tissues were dehydrated in 70% ethanol followed by paraffin processing. The lungs were cut into 4–5 μm thick sections, stained with H&E, and determined by light microscopy. Lung injury scores were evaluated by an investigator blinded to the treatment groups using the histological semiquantitative scoring system as described previously (27).

Statistics

All values are expressed as means ± SD. One-way ANOVA and Student Newman–Keuls test for post hoc comparisons were used to test differences between the means of three or more groups. Mann-Whitney U test was performed to detect significant differences between two experimental groups. The Spearman-rank correlation was applied to determine the correlation. A $p<0.05$ was considered statistically significant.

Results

Depletion of Rab1a abolishes release of IL-1β and IL-18 by murine BMDMs

To investigate the potential role of Rab1a in the regulation of the secretion of IL-1β and IL-18, Rab1a expression in BMDMs was genetically manipulated by transfection with a range of siRNA concentrations (0, 5, 10, and 20 nM) which depleted Rab1a to three levels (~50, 20, and 5%, respectively) (Fig. 1A and Supplemental Fig. 1). We observed a positive correlation between the generation of mature 17-kDa IL-1β and 18-kDa IL-18 in media and the level of Rab1a protein expression in response to ATP stimulation after LPS priming (Fig. 1A and Supplemental Fig. 1). Depletion of Rab1a by siRNA also reduced LPS/ATP-induced active caspase-1 production and NLRP3 expression (Fig. 1A). The changes in IL-1β and IL-18 in the cell culture medium following Rab1a depletion were verified by ELISA assay (Fig. 1B). Interestingly, we observed less intracellular pro-IL-1β and pro-IL-18 protein expression in BMDMs transfected with Rab1a siRNA (Fig. 1A and Supplemental Fig. 1). Since ATP stimulation is known to induce pyroptosis which results in processing and release of IL-1β and IL-18 in LPS-primed macrophages (6), we measured LDH in the culture supernatants of macrophages to quantify cell death. As expected, low levels of LDH were present in the culture supernatants of BMDMs stimulated with LPS, whereas higher concentrations of LDH were observed in LPS-primed macrophages stimulated with ATP (Fig. 1C). However, depletion of Rab1a by a specific siRNA did not alter LDH release in macrophages stimulated with LPS alone or in combination with ATP, relative to sufficient Rab1a (Fig. 1C), suggesting that the release of IL-1β and IL-18 induced by Rab1a expression is not from cell injury. Our results indicate that Rab1a positively regulates the secretion of mature IL-1β and IL-18 as well as the expression of pro-IL-1β and pro-IL-18 in murine BMDMs.

Inactivation of Rab1a abolishes release of IL-1β and IL-18 by murine BMDMs.

Rab GTPases switch between an inactive GDP-bound state and an active GTP-bound state (11). Next, we examined whether GTP/GDP-dependent activity of Rab1a is required for the release of IL-1β and IL-18. As shown in Figure 2A and Supplemental Fig. 2A, the levels of GTP-Rab1a in BMDMs following LPS stimulation increased, peaked at 5 min and thereafter decreased gradually. To determine the role of Rab1a activity in regulating the release of IL-1β and IL-18, BMDMs were transfected with Flag-tagged wild-type Rab1a (Rab1a WT) or dominant negative guanine nucleotide binding–deficient mutant Rab1a N124I plasmid (Fig. 2B). Macrophages expressing Rab1a WT showed increased production of IL-1β and IL-18 from LPS-primed BMDMs following ATP stimulation whereas expression of Rab1a N124I dramatically decreased the release of IL-1β and IL-18 (Fig. 2B and Supplemental Fig. 2B). A similar pattern was seen in the expression of pro-IL-1β and pro-IL-18 in

macrophages expressing Rab1a WT and Rab1a N124I either in the presence of LPS alone or combined with ATP. The changes in the release of IL-1β and IL-18 in macrophages expressing different Rab1a were also confirmed by ELISA assay (Fig. 2C). Similarly, exogenous expression of Rab1a WT or Rab1a N124I had no effect on LDH release in macrophages stimulated with LPS or combined with ATP as compared with control cells transfected with empty vector (Fig. 2D), indicating that Rab1a-induced change in the levels of IL-1β/IL-18 in the medium did not result from cell damage. Thus, Rab1a activity serves an important role in the release of IL-1β and IL-18 in macrophages in response to stimulation with LPS and ATP.

Rab1a activation stimulates NF-κB signaling for up-regulation of pro-IL-1β and pro-IL-18

The above studies showed that reduced release of IL-1β and IL-18 by inactivation of Rab1a in macrophages was at least partially due to the decreased production of pro-IL-1β and pro-IL-18, respectively (Fig. 2B and Supplemental Fig. 2B). Since the expression of pro-IL-1β and pro-IL-18 is dependent on activation of NF-κB (31), we examined the role of Rab1a activity in NF-κB pathway. As expected, LPS induced an increase in phosphorylation (activation) of NF-κB subunit p-65 and inhibitory IκBα subunit degradation in BMDMs transduced with vector. However, expression of Rab1a N124I abolished LPS-induced p-65 phosphorylation and IκBα degradation whereas overexpression of Rab1a WT enhanced the phosphorylation of p-65 and the degradation of inhibitory IκBα subunit (Fig. 3A). Inhibition of NF-κB activation with the highly selective IκB kinase inhibitor BMS-345541 (32) greatly attenuated Rab1a WT expression-induced enhancement in pro-IL-1β and pro-IL-18 (Fig. 3B and Supplemental Fig. 3) as well as the secretion of IL-1β and IL-18 (Fig. 3C) in response to ATP stimulation after LPS priming. These results indicate that Rab1a activation is required for LPS-induced NF-κB activation which leads to an increase in the expression of pro-IL-1β and pro-IL-18 and subsequent release of IL-1β and IL-18 by macrophages.

Rab1a up-regulates surface expression of TLR4

LPS signals through TLR4 to induce NF-κB activation (33). The total and/or surface expressions of TLR4 are required for TLR4/NF-κB signaling (34). We thus determined whether Rab1a could modulate total TLR4 expression. Immunoblotting analysis indicated that expression of Rab1a WT or Rab1a N124I did not alter the total levels of TLR4 protein following LPS stimulation in BMDMs (Fig. 4A). However, flow-cytometry analysis showed that inactivation by expression of Rab1a N124I decreased, while overexpression of Rab1a WT significantly increased TLR4 surface expression in unstimulated cells compared with control vector-transfected macrophages (Figs. 4B and 4C). Upon LPS stimulation, TLR4 surface expression was decreased in BMDMs transfected with vector, Rab1a WT or Rab1a N124I (Figs. 4B and 4C). To further determine the mechanisms by which Rab1a regulates TLR4 surface expression following LPS stimulation, we used membrane protein biotinylation to study TLR4 internalization (19). Biotinylated cell surface TLR4 proteins (Fig. 4D, lane 1, 4 and 7) were precipitated using streptavidin-agarose beads. Following LPS stimulation, approximately 30% of total biotinylated TLR4 was detected in the cytoplasm (Fig. 4D, lane 3, 6 and 9), indicating that surface TLR4 was substantially internalized and hence protected from stripping. Endocytosis rates of TLR4 in BMDMs transfected with vector, Rab1a WT or Rab1a N124I were similar after LPS treatment (Fig. 4D). Further

analysis demonstrated that TLR4 was predominantly accumulated in the ER (marker PDI) in BMDMs transfected with Rab1a N124I compared with that in BMDMs transfected with vector and Rab1a WT (Fig. 4E). These data suggest that Rab1a activation following LPS stimulation promotes the cell-surface expression of TLR4 through modulating TLR4 traffic from the ER to the cell membrane.

Rab1a activates NLRP3 inflammasome through mitochondrial ROS signaling

The amount of IL-1β and IL-18 secretion depends on not only the production of pro-IL-1β and pro-IL-18, but also inflammasome–dependent activation of caspase-1 for cleavage of these precursors (7). We thus examined whether Rab1a regulated NLRP3 activation and observed that inactivation of Rab1a by expression of Rab1a N124I markedly inhibited active caspase-1 production and NLRP3 expression in LPS-primed BMDMs stimulated with ATP, whereas overexpression of Rab1a enhanced the production of caspase-1 and NLRP3 expression compared with vector control (Fig. 5A). In NLRP3 inflammasomes, ASC must be oligomerized to recruit pro-caspase-1 for the activation of caspase-1 (35–37). Our results revealed that expression of Rab1a N124I in LPS-primed BMDMs greatly decreased, while overexpression of Rab1a increased, ATP-induced ASC oligomerization (Fig. 5B). Since mitochondrial ROS are essential for NLRP3 inflammasome activation (35), we evaluated the role of mitochondrial ROS. Treatment of macrophages with the mitochondria-targeted ROS scavenger Mito-TEMPO (38, 39) abolished the release of IL-1β and IL-18 in LPS-primed BMDMs transfected with Rab1a WT (Fig. 5C), demonstrating that Rab1a activates NLRP3 inflammasome via mitochondrial ROS signaling.

Rab1a regulates mitochondrial ROS production through modulation of cytochrome c oxidase

CcO catalyzes the final step in mitochondrial electron transfer chain from reduced cytochrome c to molecular oxygen to form H_2O. Deficiency in the expression and activity of CcO results in mitochondrial ROS production (40, 41). In the present study, there was no difference in CcO protein expression in BMDMs transfected with vector, Rab1a WT or Rab1a N124I cDNA either in the absence or presence of LPS and ATP stimulation (Fig. 6A). However, stimulation of BMDMs with LPS/ATP significantly reduced the activity of CcO which is further decreased in macrophages transfected with Rab1a WT cDNA. This decrease in the activity of CcO was reversed by expression of Rab1a N124I (Fig. 6B). Furthermore, expression of Rab1a N124I markedly inhibited the production of mitochondrial ROS in LPS-primed BMDMs stimulated with ATP, whereas overexpression of Rab1a enhanced the production of mitochondrial ROS compared with vector control (Fig. 6C). These findings indicate that Rab1a activation suppresses CcO activity, leading to increased mitochondrial ROS production. Protein interaction database shows that Rab1 interacts with CcO in *Drosophila melanogaster* (42). To further explore the mechanism by which Rab1a regulates CcO activity, we examined the possibility of the interaction between Rab1a and CcO in BMDMs. The association of Rab1a and CcO was detected in untreated BMDMs and increased in LPS-primed macrophages stimulated with ATP. Expression of Rab1a N124I prevented the association of Rab1a with CcO whereas overexpression of Rab1a increased this association (Fig. 6D). The colocalization of Rab1a and CcO were also detected in unstimulated control cells and increased in LPS-primed BMDMs stimulated with

ATP. Expression of Rab1a N124I blocked the colocalization of Rab1a and CcO whereas overexpression of Rab1a WT promoted this colocalization (Fig. 6E). These results suggest that Rab1a activation up-regulates mitochondrial ROS production via inactivation of CcO by its association with CcO.

Rab1a inactivation in macrophages dramatically attenuates polymicrobial sepsis-induced lung injury

Using an established *in vivo* model (27, 43), we next determined whether macrophage Rab1a activation plays an essential role in lung inflammation and injury. Mice were depleted of alveolar macrophages (Supplemental Fig. 4) and then received BMDMs that were transfected with dominant negative Rab1a N124I cDNA to specifically inactivate Rab1a. At 0.5 h after BMDM transplantation, mice were challenged with CLP or sham surgery (Fig. 7A). As described in our previous publications (27), the spatial distribution of macrophages in alveolar macrophage–depleted lungs receiving BMDMs is uniform and comparable among different groups. Total cell counts (Fig. 7B), PMN counts in BALF (Fig. 7C), lung MPO levels (Fig. 7D), protein level in BALF (Fig. 7E), and leakage of Evans blue dye (Fig. 7F) significantly elevated in control mice (without alveolar macrophage depletion) challenged with CLP. Mice depleted of alveolar macrophages showed less PMN infiltration (Figs. 7C, 7D), exuded protein (Fig. 7E), and leakage of Evans blue dye (Fig. 7F) following CLP challenge, whereas these responses were reversed by administration of control empty vector-transfected BMDMs (Figs. 7C–7F), consistent with our previous findings (19, 27, 43). Alveolar macrophage–depleted mice receiving Rab1a WT-transfected BMDMs showed further increased PMN counts in BAL fluid (Fig. 7C), lung MPO (Fig. 7D), protein levels in BAL fluid (Fig. 7E), and leakage of Evans blue dye (Fig. 7F) compared with mice receiving vector-transfected BMDMs following CLP challenge. Importantly, these responses were markedly attenuated in alveolar macrophage–depleted mice receiving Rab1a N124I-transfected BMDMs. Lung tissues from control mice (without alveolar macrophage depletion) challenged with CLP were presented with severe histological changes, including alveolar congestion, exudates, and infiltration of inflammatory cells, in comparison with shamed mice (Fig. 7G). These histopathological alterations in lung tissues were ameliorated in alveolar macrophage–depleted mice challenged with CLP and reversed by administration of control BMDMs, as seen in the significantly reduced lung injury score (Fig. 7G). Consistently, alveolar macrophage–depleted mice receiving Rab1a WT BMDMs exhibited worse lung inflammation and injury compared with alveolar macrophage–depleted mice receiving control BMDMs, whereas alveolar macrophage–depleted mice receiving Rab1a N124I BMDMs showed improved lung inflammation (Fig. 7G). The levels of caspase-1 (Fig. 7H), IL-1β and IL-18 (Fig. 7I) in BALF were higher in alveolar macrophage–depleted mice receiving Rab1a WT BMDMs than those in alveolar macrophage–depleted mice receiving control BMDMs. However, administration of Rab1a N124I BMDMs significantly blocked CLP-induced increase in caspase-1 (Fig. 7H), IL-1β and IL-18 (Fig. 7I) in alveolar macrophage–depleted mice receiving control or Rab1a WT BMDMs. Our results suggest that macrophage Rab1a regulates CLP-induced the release of IL-1β and IL-18 and lung inflammatory injury.

Rab1a activity in alveolar macrophages is associated with the levels of IL-1β and IL-18 in the lung and respiratory failure in ARDS patients

To determine the potential role of macrophage Rab1a in inflammatory diseases, we strictly recruited 10 patients with sepsis and 10 nonseptic controls (Table 1). Compared with the controls, the activity of Rab1a in alveolar macrophages isolated from septic patients was significantly higher while total Rab1a protein expression in alveolar macrophages was not altered (Figs. 8A and 8B). Interestingly, the levels of Rab1a activity in alveolar macrophages strongly and positively correlated with the release of IL-1β and IL-18 in the lung (Figs. 8C and8D). Moreover, Rab1a activity was negatively associated with PaO_2/FiO_2 (Fig. 8E) and positively correlated with APACHE II scores (Fig. 8F). These results demonstrate the importance of macrophage Rab1a in lung inflammatory injury.

Discussion

Dysregulation of Rab1 expression and activation has been linked to a myriad of human diseases such as cancer, cardiomyopathy, Parkinson's disease and infections (11). In the present study, our findings from the combination of primary macrophages, mouse model, and clinical study have provided strong evidence that Rab1a activation is crucial for the production of proinflammatory cytokines IL-1β and IL-18 in macrophages and subsequent lung inflammatory injury during sepsis. Rab1a regulates the release of IL-1β and IL-18 via 1) priming macrophages by up-regulating pro-IL-1β and pro-IL-18 expression and 2) activating NLRP3 inflammasome by generating mitochondrial ROS. Because the levels of Rab1a activity in alveolar macrophages strongly correlated with the severity of sepsis and respiratory failure, Rab1a may serve as a biomarker and a novel therapeutic target of sepsis-induced lung inflammatory injury.

The synthesis of the precursors pro-IL-1β and pro-IL-18 is initiated and transcriptionally regulated by NF-κB (31). Engagement of TLR4 by bacterial products leads to NF-κB activation (44). Rab7b, Rab10 and Rab11a have been reported to be involved in TLR4 signaling pathway (23, 45, 46). In this study, our results clearly support the notion that Rab1a stimulates TLR4-dependent NF-κB activation and subsequent pro-IL-1β and pro-IL-18 expression. TLR4 expression on plasma membrane is determined by the balance between TLR4 internalization and continuous replenishment of TLR4 from intracellular compartments ER, Golgi and endosomes (34). Our data indicate that Rab1a inactivation significantly reduced cell surface expression of TLR4 without altering total expression and internalization of the receptor. Further analysis demonstrated that Rab1a inactivation induced extensive accumulation of TLR4 in the ER of macrophages, consistent with the known function of Rab1 in regulating the protein trafficking specifically from the ER to Golgi apparatus (11). In addition, loss of Rab1a activity prevented NF-κB activation in LPS-stimulated macrophages. Finally, inhibition of NF-κB activation abolished the expression of pro-IL-1β and pro-IL-18 as well as the release of IL-1β and IL-18 in BMDMs overexpressing Rab1a in response to ATP stimulation after LPS priming. Taken together, these results support an essential role of Rab1a in regulating TLR4/NF-κB signaling and the release of IL-1β and IL-18 by promoting TLR4 trafficking to the cell surface en route from the ER.

The release of mature and biologically active IL-1β and IL-18 is dependent on inflammasome-mediated activation of caspase-1 that cleaves pro-IL-1β and pro-IL-18 (47). In this study, we observed that decreased secretion of IL-1β and IL-18 was coupled to a reduction in NLRP3 expression, ASC oligomerization, and caspase-1 activation in Rab1a-inactivated macrophages. These results indicate that Rab1a enhances the assembly of the inflammasome component ASC in macrophages to enable recruitment of NLRP3 and thus amplify caspase-1 activation (37) along with production of mature IL-1β and IL-18 in response to LPS priming and ATP stimulation. However, further studies are required to elucidate the exact mechanisms of how Rab1a facilitates ASC oligomerization to activate NLRP3 inflammasome. It has been shown that phosphorylation of ASC at Tyr144 by JNK and Syk is critical for the oligomerization step in response to NLRP3 stimulation (48). It is likely that Rab1a activates Syk and/or JNK through ROS signaling (49) to induce phosphorylation of ASC.

The generation of mitochondrial ROS due to mitochondrial dysfunction is considered crucial for NLRP3 inflammasome activation (39, 50). The role of mitochondrial ROS in Rab1a-mediated NLRP3 inflammasome activation is supported by data showing that a specific mitochondria ROS scavenger Mito-TEMPO abrogated the up-regulation of IL-1β and IL-18 generation in BMDMs overexpressing Rab1a in response to LPS priming and ATP stimulation. Mitochondrial CcO acts as the terminal enzyme system of the respiratory chain. Accumulating evidence points to a central role for CcO in regulating mitochondrial ROS production (40, 41). Activation of CcO induces more efficient mitochondrial coupling and inhibits mitochondrial ROS generation by strengthening electron flux capacity of the electron transport chain (25, 51, 52). A previous study showed that bacterial LPS upregulated CcO expression in murine macrophage cell lines (53). In contrast, our results demonstrated that LPS stimulation did not alter CcO expression, but instead decreased the level of CcO activity in BMDMs following LPS stimulation. Furthermore, overexpression of Rab1a decreased CcO activity in LPS-primed BMDMs stimulated with ATP while inactivation of Rab1a completely restored CcO activity. These responses are mostly likely linked to the stimulating effects of Rab1a activation on mitochondrial ROS production. Data from coimmunoprecipitation and confocal imaging further showed that the association and colocalization of Rab1a and CcO is greater in BMDMs overexpressing Rab1a and much less in cells expressing inactivated Rab1a in response to LPS priming and ATP stimulation. Thus, these findings, combined with others (25, 51, 52), support the model that Rab1a inhibits CcO activity via interacting with CcO and thus promotes mitochondrial ROS production which induces NLRP3-dependent release of IL-1β and IL-18 in macrophages. The exact mechanisms by which Rab1a regulates CcO activity require further investigation.

In summary, the current study uncovers a previously unidentified function of Rab1a in the proinflammatory response during sepsis. Our work provides the first evidence that Rab1a is a powerful regulator of the release of proinflammatory cytokines IL-1β and IL-18 in macrophages. Rab1a stimulates TLR4/NF-κB signaling by promoting TLR4 trafficking from ER to cell membrane and activates NLRP3 inflammasome through facilitating mitochondrial ROS generation (Fig. 9). The data from both basic and clinical studies presented here may provide a basis for novel therapies targeting inflammasomes and inflammation-associated diseases such as sepsis.

Supplementary Material

Refer to Web version on PubMed Central for supplementary material.

Acknowledgements

We thank Maricela Castellon (Department of Anesthesiology, University of Illinois College of Medicine) for technical assistance. The authors are grateful to Baojun Yu, Wei Wang, Zhe Zhou (Department of Critical Care Medicine, Affiliated Baoan Hospital of Shenzhen, Southern Medical University) for collecting samples from patients, and Xin Liu (Central Laboratory, Affiliated Baoan Hospital of Shenzhen, Southern Medical University) for technical assistance.

This work was supported by NIH NHLBI grants HL104092 (GH) and the Natural Science Foundation of China 81470259 (GH).

Abbreviations used in this article

APACHE	Acute Physiology and Chronic Health Evaluation
ASC	adaptor apoptosis-associated speck-like protein containing a caspase recruitment domain
BALF	bronchoalveolar lavage fluid
BMDM	bone marrow–derived macrophage
CcO	Cytochrome C oxidase
CLP	cecal ligation and puncture
ER	endoplasmic reticulum
LDH	lactate dehydrogenase
MPO	myeloperoxidase
NLRP3	nucleotide-binding oligomerization domain-like receptor containing pyrin domain 3
PMN	polymorphonuclear neutrophil
Rab	Ras-related protein in brain
ROS	reactive oxygen species
siRNA	small interfering RNA
WT	wild type

References

1. Schulert GS, and Grom AA. 2015 Pathogenesis of macrophage activation syndrome and potential for cytokine- directed therapies. Annu Rev Med 66: 145–159. [PubMed: 25386930]
2. Fenini G, Contassot E, and French LE. 2017 Potential of IL-1, IL-18 and Inflammasome Inhibition for the Treatment of Inflammatory Skin Diseases. Front Pharmacol 8: 278. [PubMed: 28588486]

3. Ganter MT, Roux J, Miyazawa B, Howard M, Frank JA, Su G, Sheppard D, Violette SM, Weinreb PH, Horan GS, Matthay MA, and Pittet JF. 2008 Interleukin-1beta causes acute lung injury via alphavbeta5 and alphavbeta6 integrin-dependent mechanisms. Circ Res 102: 804–812. [PubMed: 18276918]

4. Cruz CM, Rinna A, Forman HJ, Ventura AL, Persechini PM, and Ojcius DM. 2007 ATP activates a reactive oxygen species-dependent oxidative stress response and secretion of proinflammatory cytokines in macrophages. J Biol Chem 282: 2871–2879. [PubMed: 17132626]

5. Weinberg SE, Sena LA, and Chandel NS. 2015 Mitochondria in the regulation of innate and adaptive immunity. Immunity 42: 406–417. [PubMed: 25786173]

6. Gurung P, Li B, Subbarao Malireddi RK, Lamkanfi M, Geiger TL, and Kanneganti TD. 2015 Chronic TLR Stimulation Controls NLRP3 Inflammasome Activation through IL-10 Mediated Regulation of NLRP3 Expression and Caspase-8 Activation. Sci Rep 5: 14488. [PubMed: 26412089]

7. Eder C 2009 Mechanisms of interleukin-1beta release. Immunobiology 214: 543–553. [PubMed: 19250700]

8. Lee S, Nakahira K, Dalli J, Siempos II, Norris PC, Colas RA, Moon JS, Shinohara M, Hisata S, Howrylak JA, Suh GY, Ryter SW, Serhan CN, and Choi AMK 2017 NLRP3 Inflammasome Deficiency Protects against Microbial Sepsis via Increased Lipoxin B4 Synthesis. Am J Respir Crit Care Med 196: 713–726. [PubMed: 28245134]

9. Stenmark H 2009 Rab GTPases as coordinators of vesicle traffic. Nat Rev Mol Cell Biol 10: 513–525. [PubMed: 19603039]

10. Hutagalung AH, and Novick PJ. 2011 Role of Rab GTPases in membrane traffic and cell physiology. Physiol Rev 91: 119–149. [PubMed: 21248164]

11. Yang XZ, Li XX, Zhang YJ, Rodriguez-Rodriguez L, Xiang MQ, Wang HY, and Zheng XF. 2016 Rab1 in cell signaling, cancer and other diseases. Oncogene 35: 5699–5704. [PubMed: 27041585]

12. Touchot N, Zahraoui A, Vielh E, and Tavitian A. 1989 Biochemical properties of the YPT-related rab1B protein. Comparison with rab1A. FEBS Lett 256: 79–84. [PubMed: 2509243]

13. Wang C, Yoo Y, Fan H, Kim E, Guan KL, and Guan JL. 2010 Regulation of Integrin beta 1 recycling to lipid rafts by Rab1a to promote cell migration. J Biol Chem 285: 29398–29405. [PubMed: 20639577]

14. Zoppino FC, Militello RD, Slavin I, Alvarez C, and Colombo MI. 2010 Autophagosome formation depends on the small GTPase Rab1 and functional ER exit sites. Traffic 11: 1246–1261. [PubMed: 20545908]

15. Singer M, Deutschman CS, Seymour CW, Shankar-Hari M, Annane D, Bauer M, Bellomo R, Bernard GR, Chiche JD, Coopersmith CM, Hotchkiss RS, Levy MM, Marshall JC, Martin GS, Opal SM, Rubenfeld GD, van der Poll T, Vincent JL, and Angus DC. 2016 The Third International Consensus Definitions for Sepsis and Septic Shock (Sepsis-3). JAMA 315: 801–810. [PubMed: 26903338]

16. Force ADT, Ranieri VM, Rubenfeld GD, Thompson BT, Ferguson ND, Caldwell E, Fan E, Camporota L, and Slutsky AS. 2012 Acute respiratory distress syndrome: the Berlin Definition. JAMA 307: 2526–2533. [PubMed: 22797452]

17. Maruyama M, Kawasaki A, Suzuki H, Yamashita N, and Yano S. 1990 Lysis of Human Alveolar Macrophages by Lymphokine-Activated Killer Cells. Chest 97: 1372–1376. [PubMed: 2347221]

18. Celada A, Gray PW, Rinderknecht E, and Schreiber RD. 1984 Evidence for a gamma-interferon receptor that regulates macrophage tumoricidal activity. J Exp Med 160: 55–74. [PubMed: 6330272]

19. Yang Z, Sun D, Yan Z, Reynolds AB, Christman JW, Minshall RD, Malik AB, Zhang Y, and Hu G. 2014 Differential role for p120-catenin in regulation of TLR4 signaling in macrophages. J Immunol 193: 1931–1941. [PubMed: 25015829]

20. Harris J, Hartman M, Roche C, Zeng SG, O'Shea A, Sharp FA, Lambe EM, Creagh EM, Golenbock DT, Tschopp J, Kornfeld H, Fitzgerald KA, and Lavelle EC. 2011 Autophagy controls IL-1beta secretion by targeting pro-IL-1beta for degradation. J Biol Chem 286: 9587–9597. [PubMed: 21228274]

21. Shi H, Wang Y, Li X, Zhan X, Tang M, Fina M, Su L, Pratt D, Bu CH, Hildebrand S, Lyon S, Scott L, Quan J, Sun Q, Russell J, Arnett S, Jurek P, Chen D, Kravchenko VV, Mathison JC, Moresco EM, Monson NL, Ulevitch RJ, and Beutler B. 2016 NLRP3 activation and mitosis are mutually exclusive events coordinated by NEK7, a new inflammasome component. Nat Immunol 17: 250–258. [PubMed: 26642356]
22. Yan Z, Wang ZG, Segev N, Hu S, Minshall RD, Dull RO, Zhang M, Malik AB, and Hu G. 2016 Rab11a Mediates Vascular Endothelial-Cadherin Recycling and Controls Endothelial Barrier Function. Arterioscler Thromb Vasc Biol 36: 339–349. [PubMed: 26663395]
23. Husebye H, Aune MH, Stenvik J, Samstad E, Skjeldal F, Halaas O, Nilsen NJ, Stenmark H, Latz E, Lien E, Mollnes TE, Bakke O, and Espevik T. 2010 The Rab11a GTPase controls Toll-like receptor 4-induced activation of interferon regulatory factor-3 on phagosomes. Immunity 33: 583–596. [PubMed: 20933442]
24. Lin YC, Huang DY, Wang JS, Lin YL, Hsieh SL, Huang KC, and Lin WW. 2015 Syk is involved in NLRP3 inflammasome-mediated caspase-1 activation through adaptor ASC phosphorylation and enhanced oligomerization. J Leukoc Biol 97: 825–835. [PubMed: 25605870]
25. Oliva CR, Nozell SE, Diers A, McClugage SG, 3rd, Sarkaria JN, Markert JM, Darley-Usmar VM, Bailey SM, Gillespie GY, Landar A, and Griguer CE. 2010 Acquisition of temozolomide chemoresistance in gliomas leads to remodeling of mitochondrial electron transport chain. J Biol Chem 285: 39759–39767. [PubMed: 20870728]
26. Dadson K, Hauck L, Hao Z, Grothe D, Rao V, Mak TW, and Billia F. 2017 The E3 ligase Mule protects the heart against oxidative stress and mitochondrial dysfunction through Myc-dependent inactivation of Pgc-1alpha and Pink1. Sci Rep 7: 41490. [PubMed: 28148912]
27. Jiang C, Liu Z, Hu R, and Bo L. 2017 Inactivation of Rab11a GTPase in Macrophages Facilitates Phagocytosis of Apoptotic Neutrophils. J Immunol 198: 1660–1672. [PubMed: 28053235]
28. Cauvi DM, Song D, Vazquez DE, Hawisher D, Bermudez JA, Williams MR, Bickler S, Coimbra R, and De Maio A. 2012 Period of irreversible therapeutic intervention during sepsis correlates with phase of innate immune dysfunction. J Biol Chem 287: 19804–19815. [PubMed: 22518839]
29. Wu J, Yan Z, Schwartz DE, Yu J, Malik AB, and Hu G. 2013 Activation of NLRP3 inflammasome in alveolar macrophages contributes to mechanical stretch-induced lung inflammation and injury. J Immunol 190: 3590–3599. [PubMed: 23436933]
30. Moitra J, Sammani S, and Garcia JG. 2007 Re-evaluation of Evans Blue dye as a marker of albumin clearance in murine models of acute lung injury. Transl Res 150: 253–265. [PubMed: 17900513]
31. Bauernfeind FG, Horvath G, Stutz A, Alnemri ES, MacDonald K, Speert D, Fernandes-Alnemri T, Wu J, Monks BG, Fitzgerald KA, Hornung V, and Latz E. 2009 Cutting edge: NF-kappaB activating pattern recognition and cytokine receptors license NLRP3 inflammasome activation by regulating NLRP3 expression. J Immunol 183: 787–791. [PubMed: 19570822]
32. Burke JR, Pattoli MA, Gregor KR, Brassil PJ, MacMaster JF, McIntyre KW, Yang X, Iotzova VS, Clarke W, Strnad J, Qiu Y, and Zusi FC. 2003 BMS-345541 is a highly selective inhibitor of I kappa B kinase that binds at an allosteric site of the enzyme and blocks NF-kappa B-dependent transcription in mice. J Biol Chem 278: 1450–1456. [PubMed: 12403772]
33. Miller SI, Ernst RK, and Bader MW. 2005 LPS, TLR4 and infectious disease diversity. Nat Rev Microbiol 3: 36–46. [PubMed: 15608698]
34. Liaunardy-Jopeace A, and Gay NJ. 2014 Molecular and cellular regulation of toll-like receptor-4 activity induced by lipopolysaccharide ligands. Front Immunol 5: 473. [PubMed: 25339952]
35. Zhou R, Yazdi AS, Menu P, and Tschopp J. 2011 A role for mitochondria in NLRP3 inflammasome activation. Nature 469: 221–225. [PubMed: 21124315]
36. Broz P, von Moltke J, Jones JW, Vance RE, and Monack DM. 2010 Differential requirement for Caspase-1 autoproteolysis in pathogen-induced cell death and cytokine processing. Cell Host Microbe 8: 471–483. [PubMed: 21147462]
37. Lu A, Magupalli VG, Ruan J, Yin Q, Atianand MK, Vos MR, Schroder GF, Fitzgerald KA, Wu H, and Egelman EH. 2014 Unified polymerization mechanism for the assembly of ASC-dependent inflammasomes. Cell 156: 1193–1206. [PubMed: 24630722]

38. Park J, Min JS, Kim B, Chae UB, Yun JW, Choi MS, Kong IK, Chang KT, and Lee DS. 2015 Mitochondrial ROS govern the LPS-induced pro-inflammatory response in microglia cells by regulating MAPK and NF-kappaB pathways. Neurosci Lett 584: 191–196. [PubMed: 25459294]
39. Shimada K, Crother TR, Karlin J, Dagvadorj J, Chiba N, Chen S, Ramanujan VK, Wolf AJ, Vergnes L, Ojcius DM, Rentsendorj A, Vargas M, Guerrero C, Wang Y, Fitzgerald KA, Underhill DM, Town T, and Arditi M. 2012 Oxidized mitochondrial DNA activates the NLRP3 inflammasome during apoptosis. Immunity 36: 401–414. [PubMed: 22342844]
40. Srinivasan S, and Avadhani NG. 2012 Cytochrome c oxidase dysfunction in oxidative stress. Free Radic Biol Med 53: 1252–1263. [PubMed: 22841758]
41. Oliva CR, Markert T, Gillespie GY, and Griguer CE. 2015 Nuclear-encoded cytochrome c oxidase subunit 4 regulates BMI1 expression and determines proliferative capacity of high-grade gliomas. Oncotarget 6: 4330–4344. [PubMed: 25726526]
42. Guruharsha KG, Rual JF, Zhai B, Mintseris J, Vaidya P, Vaidya N, Beekman C, Wong C, Rhee DY, Cenaj O, McKillip E, Shah S, Stapleton M, Wan KH, Yu C, Parsa B, Carlson JW, Chen X, Kapadia B, VijayRaghavan K, Gygi SP, Celniker SE, Obar RA, and Artavanis-Tsakonas S. 2011 A protein complex network of Drosophila melanogaster. Cell 147: 690–703. [PubMed: 22036573]
43. Du X, Jiang C, Lv Y, Dull RO, Zhao YY, Schwartz DE, and Hu G. 2017 Isoflurane promotes phagocytosis of apoptotic neutrophils through AMPK-mediated ADAM17/Mer signaling. PLoS One 12: e0180213. [PubMed: 28671983]
44. Verstrepen L, Bekaert T, Chau TL, Tavernier J, Chariot A, and Beyaert R. 2008 TLR-4, IL-1R and TNF-R signaling to NF-kappaB: variations on a common theme. Cell Mol Life Sci 65: 2964–2978. [PubMed: 18535784]
45. Wang Y, Chen T, Han C, He D, Liu H, An H, Cai Z, and Cao X. 2007 Lysosome-associated small Rab GTPase Rab7b negatively regulates TLR4 signaling in macrophages by promoting lysosomal degradation of TLR4. Blood 110: 962–971. [PubMed: 17395780]
46. Wang D, Lou J, Ouyang C, Chen W, Liu Y, Liu X, Cao X, Wang J, and Lu L. 2010 Ras-related protein Rab10 facilitates TLR4 signaling by promoting replenishment of TLR4 onto the plasma membrane. Proc Natl Acad Sci U S A 107: 13806–13811. [PubMed: 20643919]
47. Martinon F, Burns K, and Tschopp J. 2002 The inflammasome: a molecular platform triggering activation of inflammatory caspases and processing of proIL-beta. Mol Cell 10: 417–426. [PubMed: 12191486]
48. Hara H, Tsuchiya K, Kawamura I, Fang R, Hernandez-Cuellar E, Shen Y, Mizuguchi J, Schweighoffer E, Tybulewicz V, and Mitsuyama M. 2013 Phosphorylation of the adaptor ASC acts as a molecular switch that controls the formation of speck-like aggregates and inflammasome activity. Nat Immunol 14: 1247–1255. [PubMed: 24185614]
49. Patterson HC, Gerbeth C, Thiru P, Vogtle NF, Knoll M, Shahsafaei A, Samocha KE, Huang CX, Harden MM, Song R, Chen C, Kao J, Shi J, Salmon W, Shaul YD, Stokes MP, Silva JC, Bell GW, MacArthur DG, Ruland J, Meisinger C, and Lodish HF. 2015 A respiratory chain controlled signal transduction cascade in the mitochondrial intermembrane space mediates hydrogen peroxide signaling. Proc Natl Acad Sci U S A 112: E5679–5688. [PubMed: 26438848]
50. Nakahira K, Haspel JA, Rathinam VA, Lee SJ, Dolinay T, Lam HC, Englert JA, Rabinovitch M, Cernadas M, Kim HP, Fitzgerald KA, Ryter SW, and Choi AM. 2011 Autophagy proteins regulate innate immune responses by inhibiting the release of mitochondrial DNA mediated by the NALP3 inflammasome. Nat Immunol 12: 222–230. [PubMed: 21151103]
51. Campian JL, Gao X, Qian M, and Eaton JW. 2007 Cytochrome C oxidase activity and oxygen tolerance. J Biol Chem 282: 12430–12438. [PubMed: 17303578]
52. Seelan RS, and Grossman LI. 1997 Structural organization and promoter analysis of the bovine cytochrome c oxidase subunit VIIc gene. A functional role for YY1. J Biol Chem 272: 10175–10181. [PubMed: 9092564]
53. Bauerfeld CP, Rastogi R, Pirockinaite G, Lee I, Huttemann M, Monks B, Birnbaum MJ, Franchi L, Nunez G, and Samavati L. 2012 TLR4-mediated AKT activation is MyD88/TRIF dependent and critical for induction of oxidative phosphorylation and mitochondrial transcription factor A in murine macrophages. J Immunol 188: 2847–2857. [PubMed: 22312125]

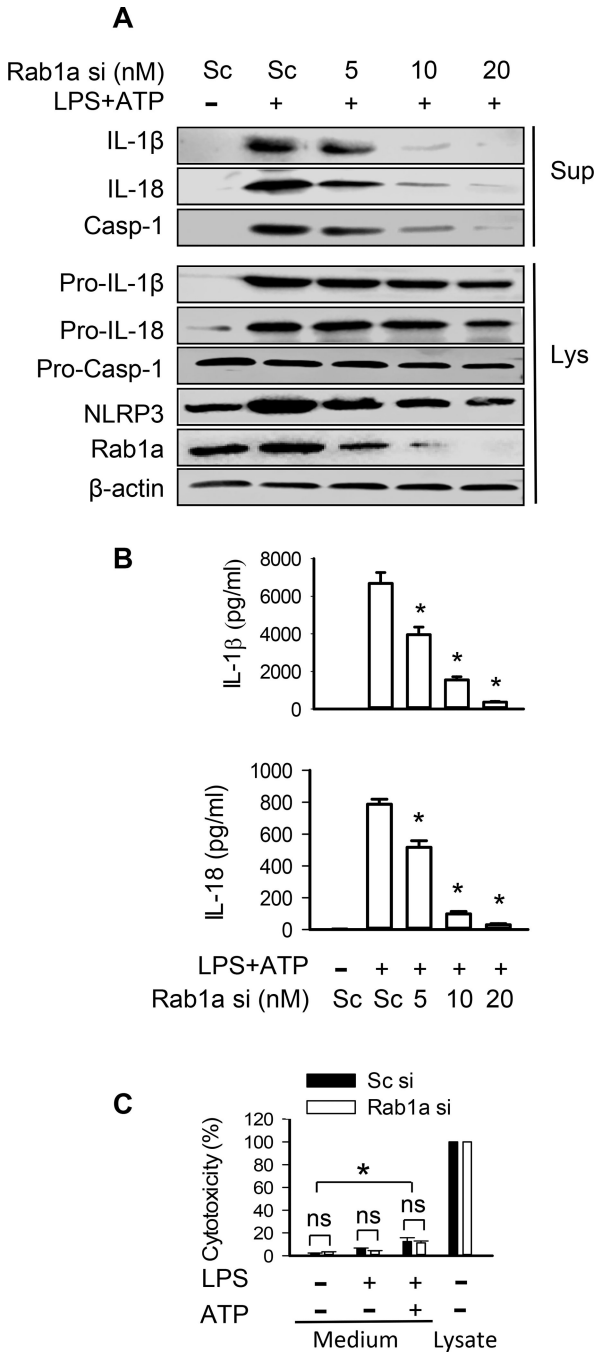

Figure 1. Depletion of Rab1a abolishes release of IL-1β and IL-18 in macrophages.

BMDMs were transfected with scrambled (Sc) or Rab1a siRNA (si) at indicated concentrations (A and B) or at a final concentration of 20 nM (C). At 48 h posttransfection, the macrophages were primed with LPS (20 ng/ ml) for 4 h and stimulated with ATP (5 mM) for 30 min. (**A**) Effects of different levels of Rab1a expression on the release of IL-1β, IL-18 and caspase-1 (Casp-1), intracellular pro-IL-1β, pro-IL-18, and pro-caspase-1. Following ATP stimulation, the release of mature IL-1β and IL-18 in the culture supernatants (Sup) of BMDMs as well as intracellular pro-IL-1β and pro-IL-18 in cell lysate (Lys) was measured

by Western blot analysis. (**B**) The levels of IL-1β and IL-18 in the culture medium were detected by ELISA. $n = 3$. *$p<0.05$, vs. control groups (LPS+ATP), Mann-Whitney test. (**C**) LDH release as a measure of cytotoxicity in LPS-primed BMDMs after ATP stimulation. Data were obtained from three independent cultures, each performed in triplicate. *$p<0.05$, Mann-Whitney test. ns = no significance.

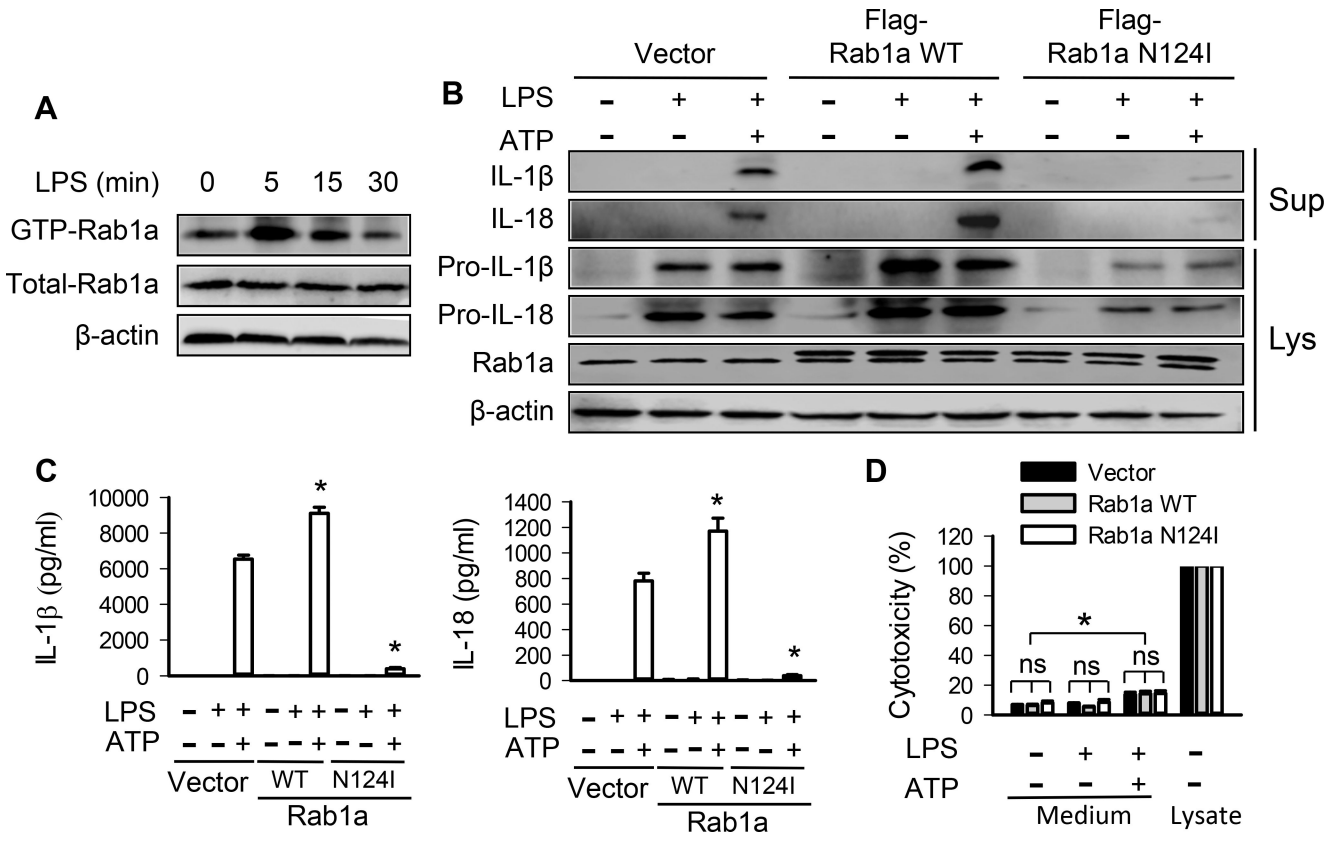

Figure 2. Inactivation of Rab1a prevents release of IL-1β and IL-18 in macrophages.

BMDMs were transfected with vector, Flag-tagged Rab1a WT or Rab1a N124I cDNA (B-D). At 48 h posttransfection, the macrophages were primed with LPS (20 ng/ ml) for 4 h and stimulated with ATP (5 mM) for 30 min. (**A**) Time-dependent Rab1a activation in BMDMs in response to LPS stimulation. BMDMs were incubated with LPS (20 ng/ ml) for the indicated time points. Pull-down experiment showed the content of Rab1-GTP. (**B**) Effects of different Rab1a expression on the release of IL-1β and IL-18 and intracellular pro-IL-1β and pro-IL-18. Following ATP stimulation, the release of mature IL-1β and IL-18 in the culture supernatants (Sup) of BMDMs as well as intracellular pro-IL-1β and pro-IL-18 expression was measured by Western blot analysis. (**C**) The levels of IL-1β and IL-18 in the culture medium were detected by ELISA. $n = 3$. *$p<0.05$, vs. vector control groups (LPS +ATP), Mann-Whitney test. (**D**) LDH release as a measure of cytotoxicity in LPS-primed BMDMs after ATP stimulation. Data were obtained from three independent cultures, each performed in triplicate. $n = 3$. *$p<0.05$, vs. control group (Vector, LPS and ATP), Mann-Whitney test. ns = no significance.

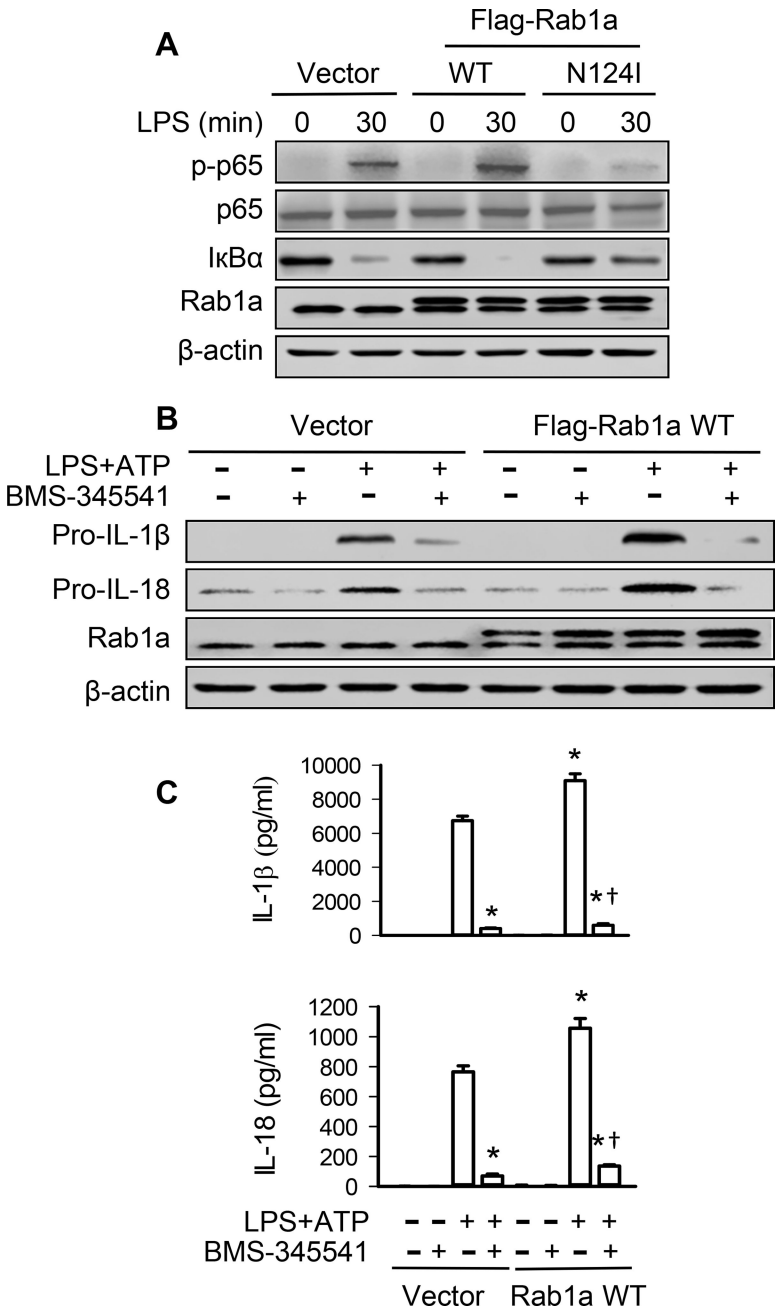

Figure 3. Rab1a regulates generation of IL-1β and IL-18 via NF-κB-dependent production of pro-IL-1β and pro-IL-18.

(**A**) Effects of expression of Rab1a WT or Rab1a N124I on IκBα degradation and NF-κB activity following LPS challenge in BMDMs. BMDMs were transfected with Flag-tagged Rab1a WT, Rab1a N124I cDNA, or control vector. At 48 h posttransfection, the macrophages were stimulated with LPS (20 ng/ ml) for 30 min. (**B**) Effects of NF-κB inhibitor on the production of pro-IL1β and pro-IL-18. BMDMs were transfected with empty vector or Flag-tagged Rab1a WT cDNA. At 48 h posttransfection, the macrophages were primed with LPS (20 ng/ ml) for 4 h and stimulated with ATP (5 mM) for 30 min in the presence of BMS-345541 (3 μM) or vehicle (PBS). (**C**) The levels of IL-1β and IL-18 in the

culture medium were detected by ELISA. Data are representative of three independent experiments. *p<0.05, vs. vector control (LPS+ATP) group; †p<0.05, vs. LPS+ATP group (Rab1a WT), one-way ANOVA.

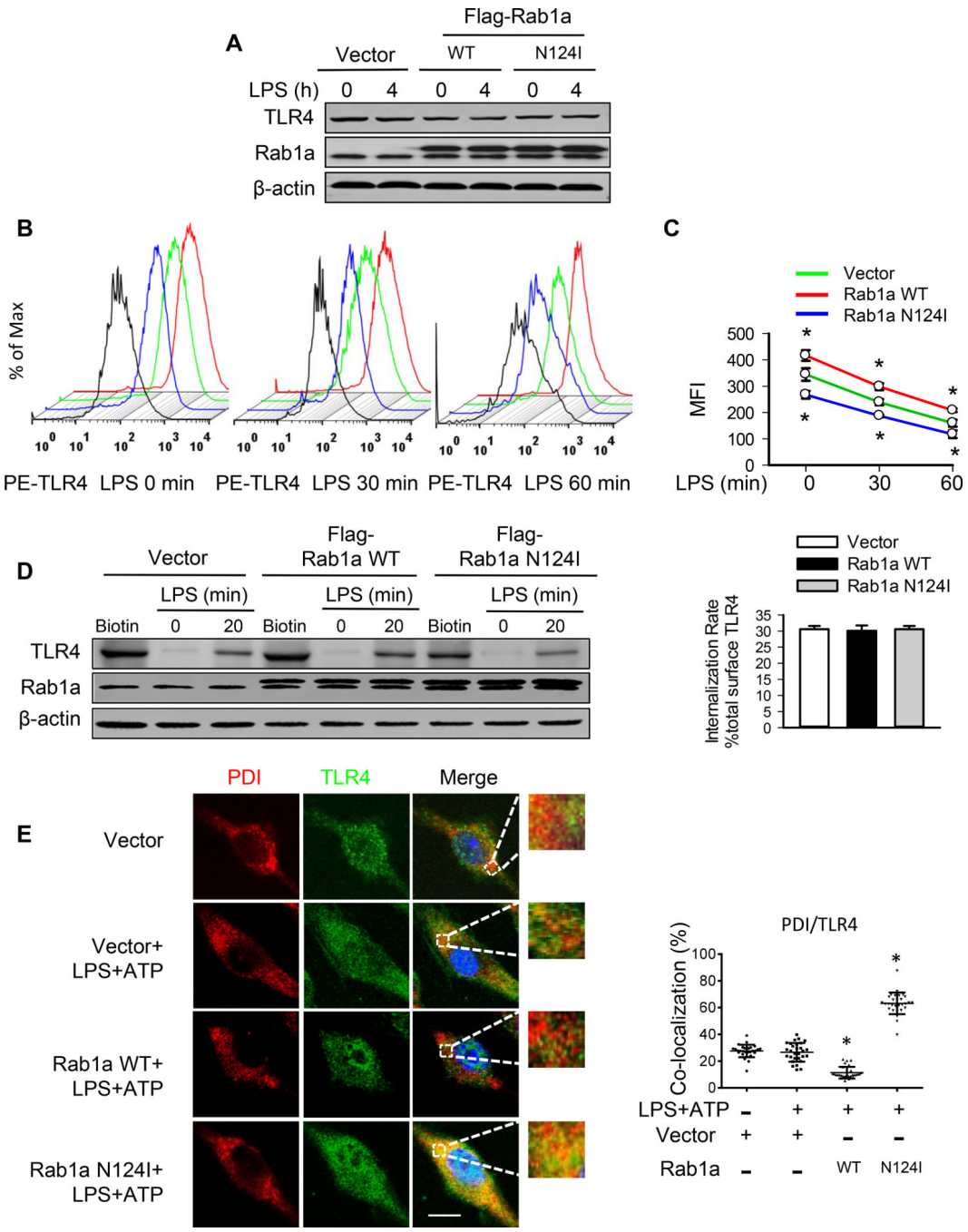

Figure 4. Rab1a induces cell surface expression of TLR4 via enhancement of TLR trafficking to plasmalemma.

BMDMs were transfected with empty vector, Flag-tagged Rab1a WT, or Rab1a N124I cDNA. At 48 h posttransfection, the macrophages were incubated with LPS (20 ng/ml) for the indicated time (A-D). (**A**) Effects of expression of Rab1a WT or Rab1a N124I on TLR4 protein expression. (**B**) Representative histograms of flow cytometry experiments demonstrating the effects of different Rab1a expression on cell surface expression of TLR4 protein in response to LPS stimulation. Cell surface expression of TLR4 protein was

evaluated using phycoerythrin (PE)-conjugated MTS510 Ab and fluorescence-activated cell sorting analysis. Black lines depict staining with irrelevant IgG2a. (**C**) Quantitative data showing changes in mean fluorescent intensity (MFI) of PE-TLR4 following LPS stimulation ($n = 3$). (**D**) Effects of different Rab1a expression on TLR4 internalization. Left panel, cell surface biotinylation of TLR4 in BMDMs; right panel, the internalization rate. (**E**) Accumulation of TLR4 in ER compartment of macrophages. Transfected macrophages were primed with LPS (20 ng/ ml) for 4 h and stimulated with ATP (5 mM) for 30 min. Subcellular distribution of TLR4 was detected by immunofluorescence for PDI (red) and TLR4 (green). Left panel, representative confocal images showing colocalization of PDI and TLR4. Bars, 10 μm. Right panel, quantification of TLR4/PDI colocalization. Results are representative of 3 independent experiments. *$p<0.05$ vs. vector control (LPS+ATP), Student *t* test.

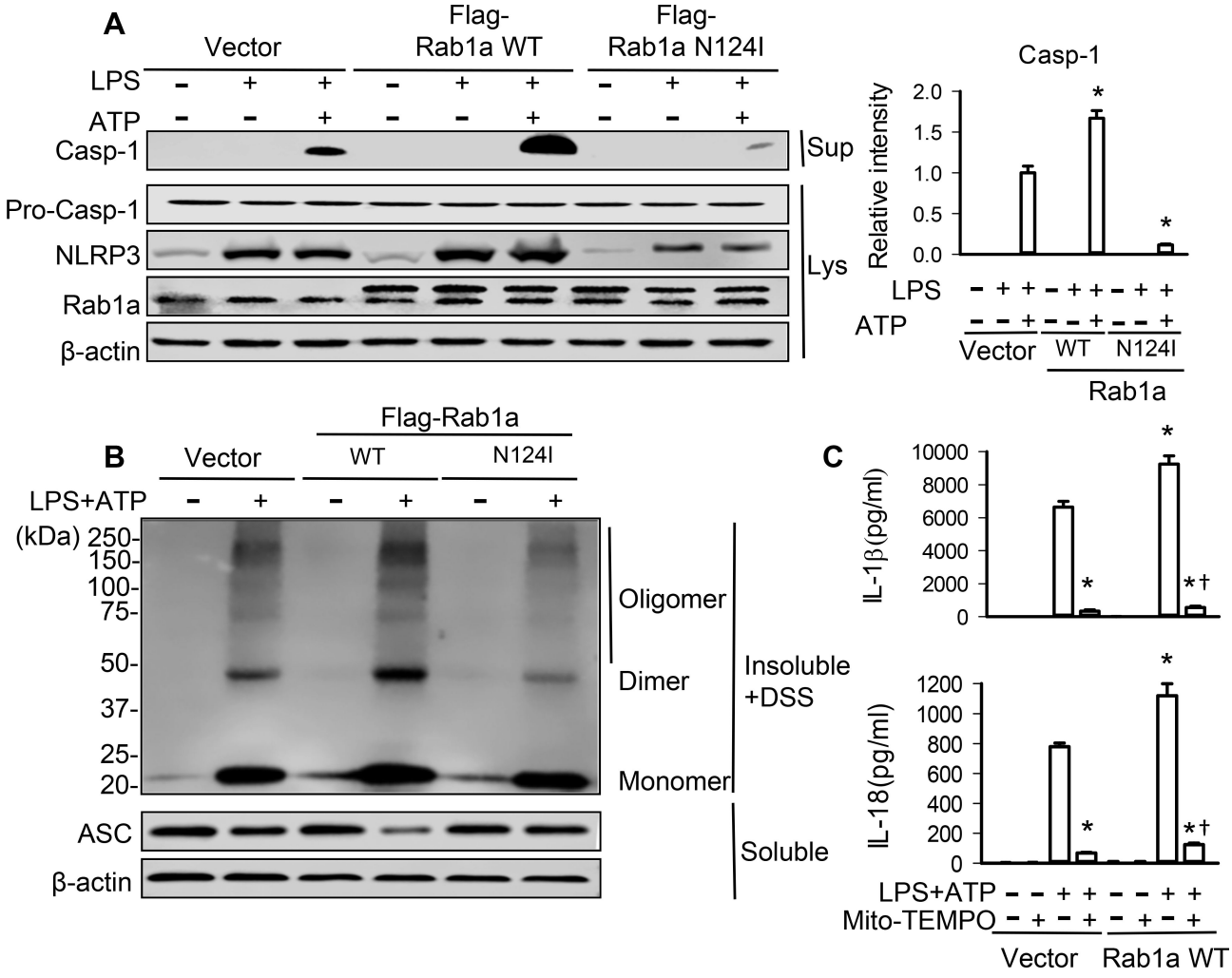

Figure 5. Rab1a regulates NLRP3 inflammasome activation through modulation of mitochondrial ROS production.

BMDMs were transfected with empty vector, Flag-tagged Rab1a WT or Rab1a N124I cDNA. At 48 h posttransfection, the macrophages were incubated with LPS (20 ng/ml) for 4 h (A) and stimulated with ATP (5 mM) for 30 min (B, C). (**A**) Effects of different Rab1a expression on the levels of caspase-1 (Casp-1). The release of Casp-1 in the culture supernatants (Sup) of BMDMs as well as pro-caspase-1 and NLRP3 in cell lysate (Lys) was measured by Western blot analysis. Left panel, representative blots showing the protein expression of caspase-1, pro-caspase-1 and NLRP3. Right panel, densitometric analysis of caspase-1 ($n = 3$ samples). The density of proteins in vector control (LPS+ATP) group was used as a standard (1 arbitrary unit) to compare relative densities in the other groups. (**B**) Effects of different Rab1a expression on ASC oligomerization. Cross-linked lysates of BMDMs were analyzed with anti-ASC immunoblotting. (**C**) IL-1β and IL-18 in cell-culture media was measured by ELISA ($n = 3$). Transfected BMDMs were pretreated with Mito-TEMPO (100 μM) for 1 h. *$p<0.05$, vs. vector control (LPS+ATP) group; †$p<0.05$, vs. corresponding WT (LPS+ATP) group, Mann-Whitney test.

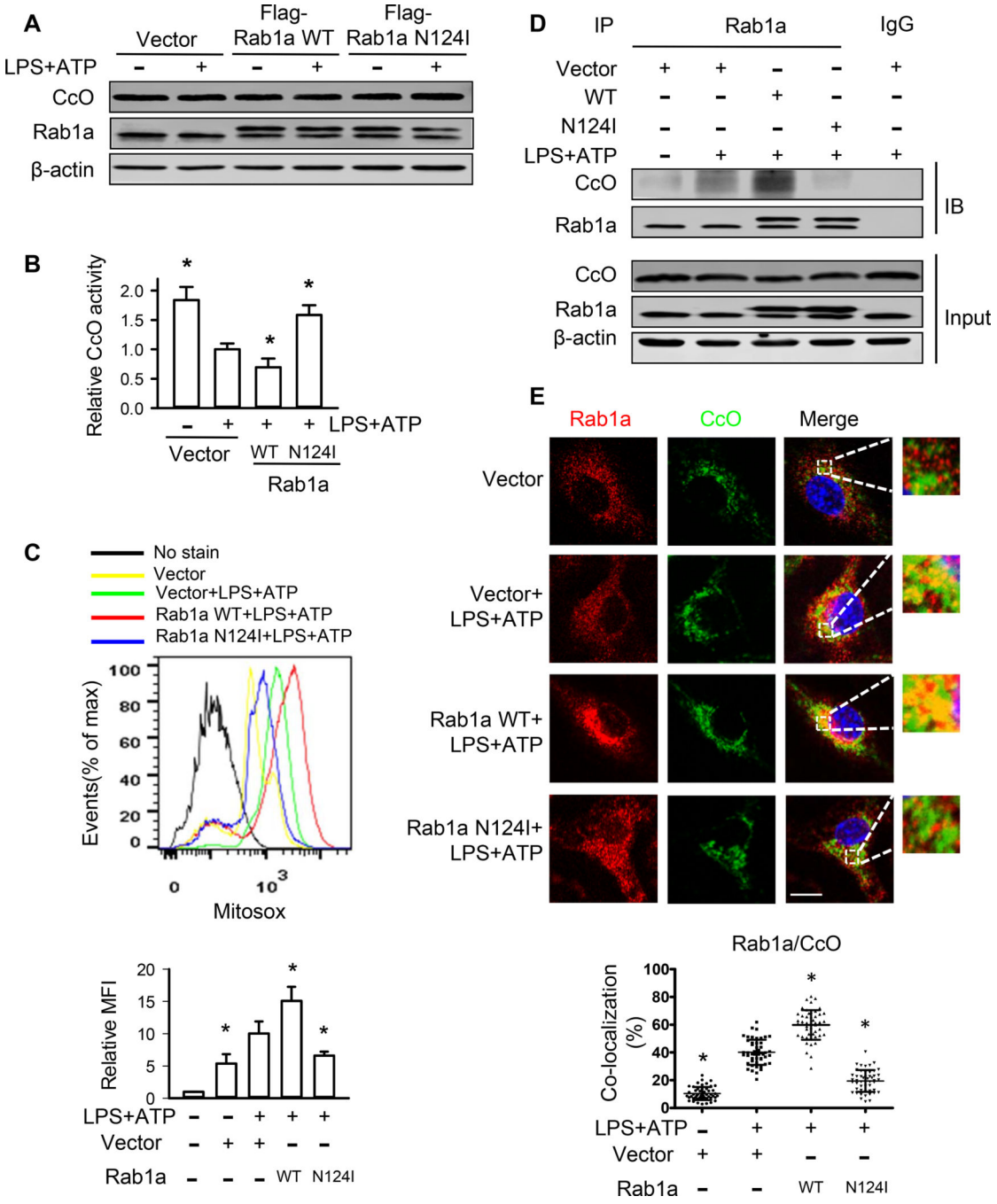

Figure 6. Rab1a inhibits CcO activation and increases mitochondrial ROS generation.

BMDMs were transfected with empty vector, Flag-tagged Rab1a WT or Rab1a N124I cDNA. At 48 h posttransfection, the macrophages were incubated with LPS (20 ng/ml) for 4 h and stimulated with ATP (5 mM) for 30 min. (**A**) Effects of different Rab1a expression on CcO protein expression. (**B**) Effects of different Rab1a expression on CcO activity. (**C**) Effects of different Rab1a expression on mitochondrial ROS production. Top panel, representative histograms of flow cytometry experiments showing mitochondrial ROS generation. Bottom panel, quantitative data showing changes in mean fluorescent intensity

(MFI) of MitoSOX ($n = 3$). (**D**) Effects of different Rab1a expression on the association of Rab1a and CcO. The association between Rab1a and CcO was detected using immunoprecipitation with anti-Rab1a Ab followed by immunoblotting for CcO. (**E**) Effects of different Rab1a expression on the colocalization of Rab1a and CcO. Top panel, representative confocal images showing colocalization of Rab1a and CcO. Bars, 10 μm. Bottom panel, quantification of Rab1a/CcO colocalization. Results are representative of 3 independent experiments. *$p<0.05$ vs. Vector with LPS+ATP group, Mann-Whitney test.

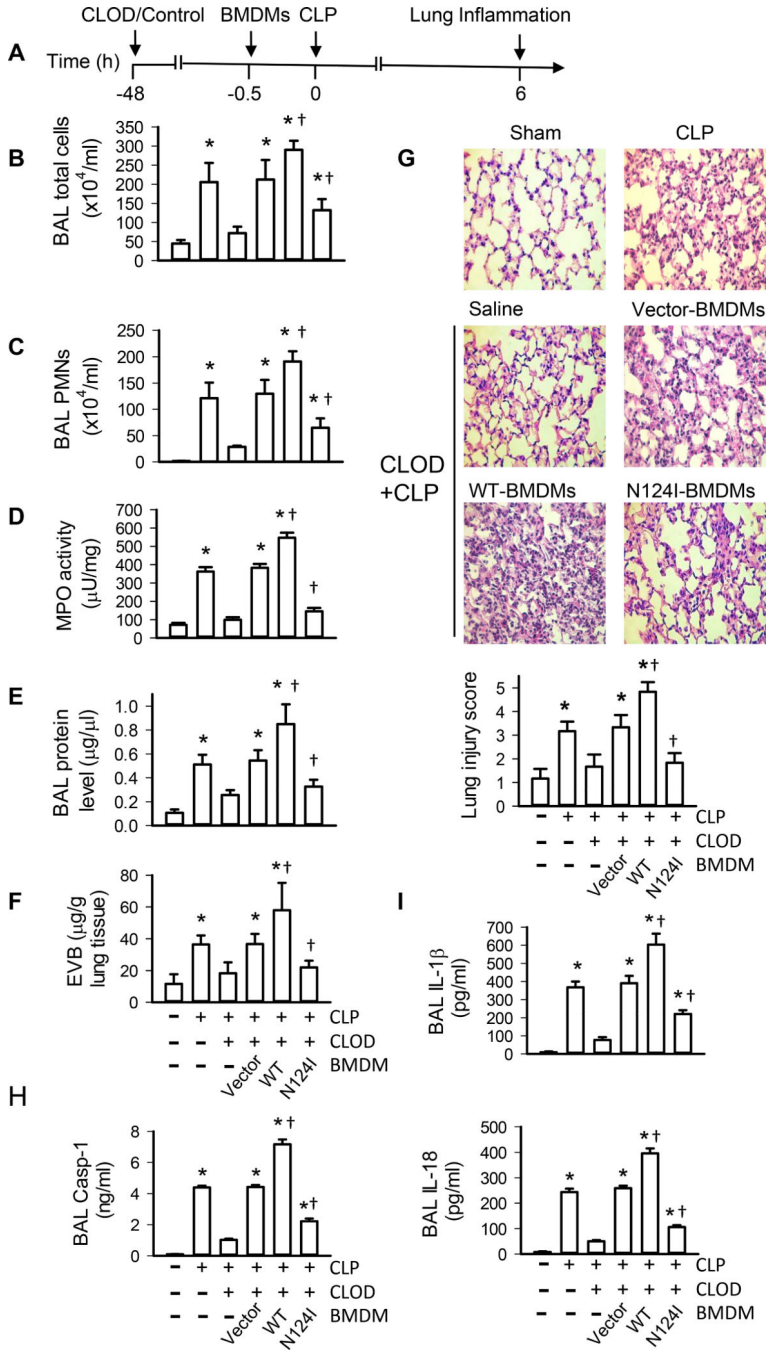

Figure 7. Role of macrophage Rab1a in lung inflammatory injury in mice.

(**A**) Experimental protocols of induction and time course of lung inflammation after CLP challenge in WT mice. Following depletion of alveolar macrophages with clodronate liposome (CLOD), mice were challenged with CLP. BMDMs isolated from donor mice were cultured and transfected with vector, Rab1a WT or Rab1a N124I cDNA. After 48 h, the efficiency of transfection was evaluated by Western blot analysis. Transfected BMDMs were i.t. injected into alveolar macrophage–depleted mice. $n = 6$ animals per group per time point. (**B**) Total cell counts in the BAL fluid. (**C**) PMN counts in the BAL fluid. (**D**) PMN

sequestration in lungs as assessed by MPO activity. (**E**) Pulmonary vascular protein permeability as determined by protein concentration of BAL fluid. (**F**) Pulmonary edema formation measured the Evans blue dye assay. (**G**) Lung histology. Top panel, histological analysis of lung tissue by H&E staining (original magnification, ×40); bottom panel, histopathological lung injury scores. Measurements were performed in triplicate for data analysis. (**H**) The levels of caspase-1 (Casp-1) in BAL fluid. (**I**) The levels of IL-1β and IL-18 in BALF determined by ELISA. *p<0.05 vs. control (without CLP) groups, †p<0.05 vs. Vector (CLOD+CLP) group, one-way ANOVA.

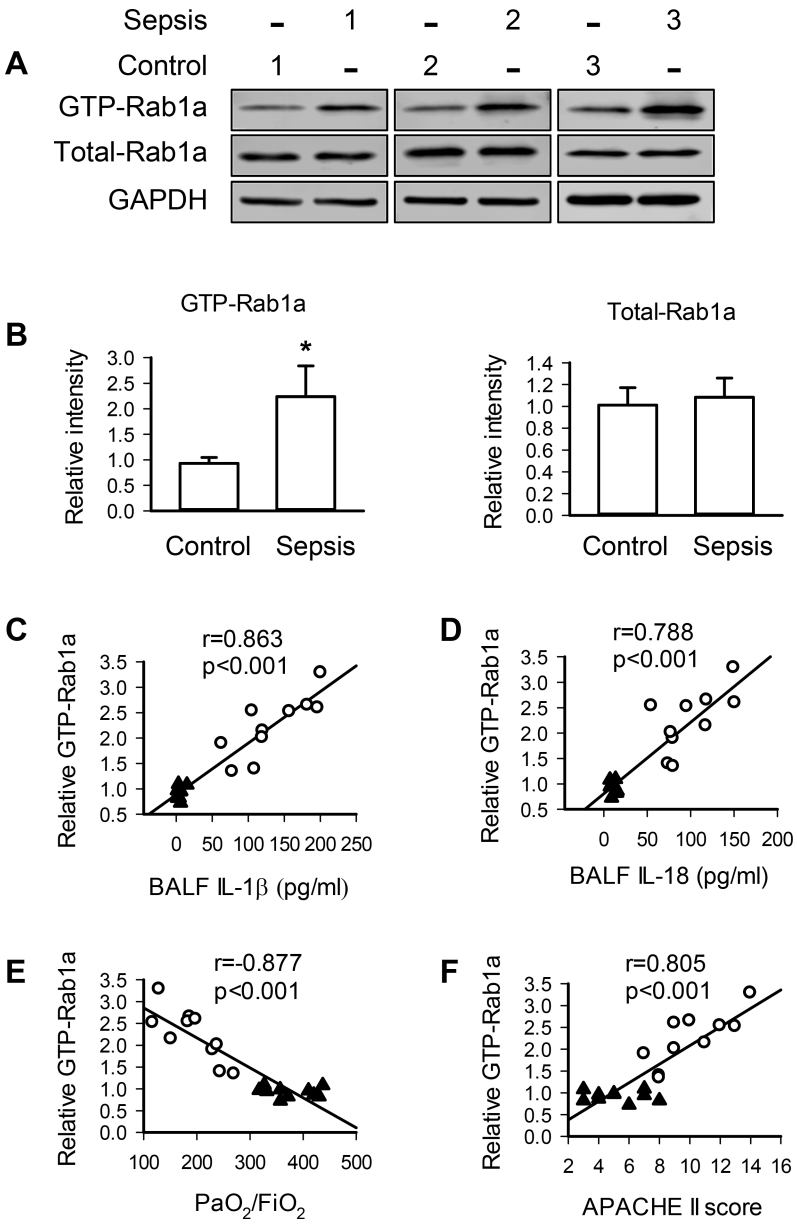

Figure 8. Rab1a activity in alveolar macrophages from patients with sepsis is associated with generation of IL-1β and IL-18 in the lung and respiratory dysfunction.

(**A**) Representative blots showing the protein expression of GTP-Rab1a and total Rab1a in alveolar macrophages from 3 different control and septic patients. (**B**) Quantification of the levels of GTP-Rab1a and total Rab1a. $n = 10$ per group. *$p<0.01$, Student t test. (**C**, **D**) Correlation of Rab1a activity in alveolar macrophages from patients with the levels of IL-1β (C) or IL-18 (D) in the lung. (**E**, **F**) Correlation of Rab1a activity with the levels of PaO_2/FiO_2 (E), and APACHE II scores (F). $n = 10$ per group. The data were analyzed by linear regression analysis with a 95% confidence interval (C-F). Open circle, septic patients; closed triangle, control (non-septic patients).

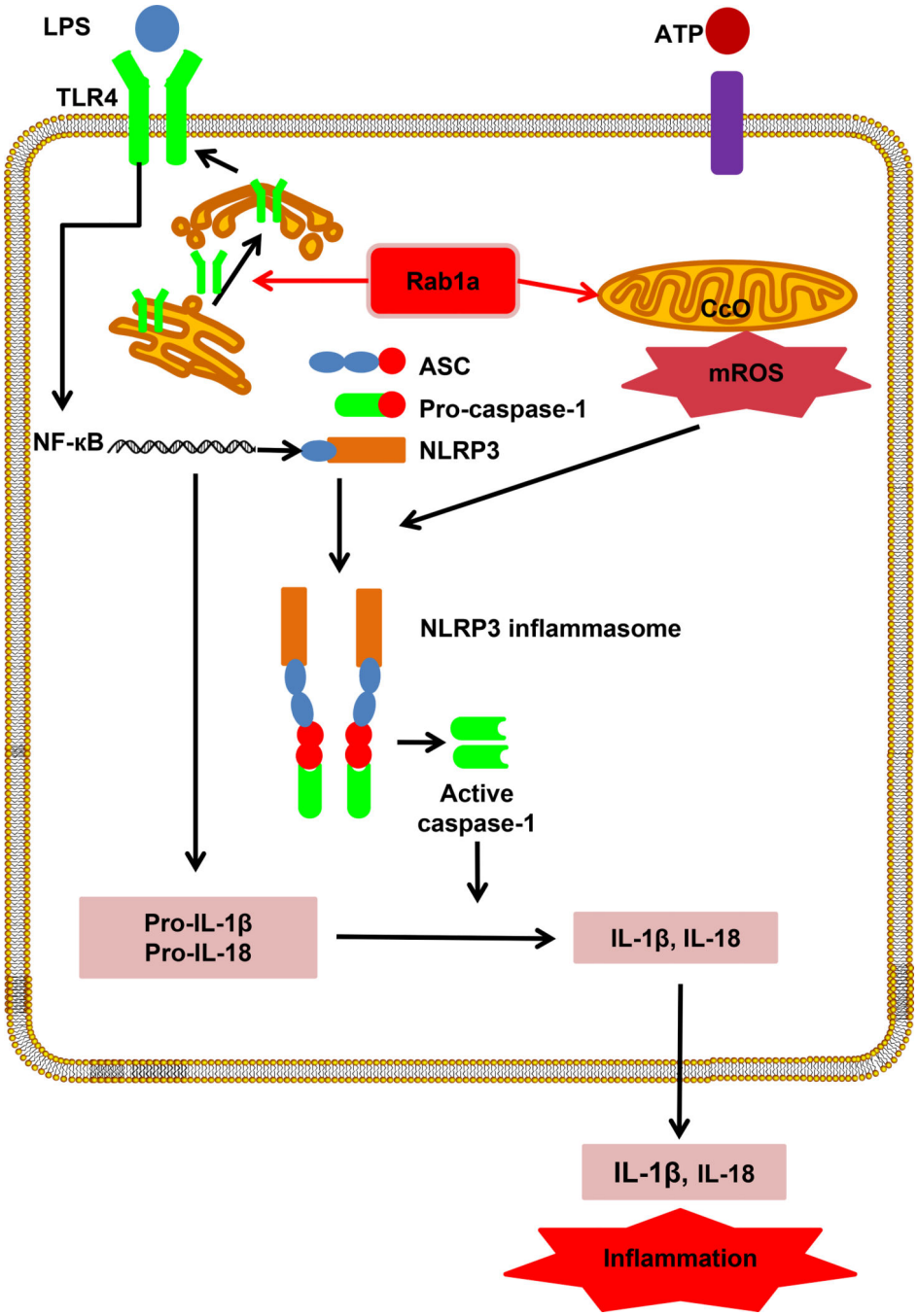

Figure 9. Model of Rab1a in regulating inflammatory response.

Abbreviation: ASC, apoptosis-associated speck-like protein containing a caspase recruitment domain; CcO, Cytochrome C oxidase; mROS, mitochondrial reactive oxygen species; NLRP3, nucleotide binding domain-like receptor family, pyrin domain containing 3; Rab, Ras-related protein in brain.

Table 1

Characteristics of control and septic patients.

Variables	Control (n=10)	Sepsis (n=10)	p value
Male	7	8	
Female	3	2	
Age (Years)	47±15.76	50.5±14.41	0.611
APACHEⅡ	5.2±1.75	10.1±2.33*	<0.001
SOFA Score	1.80±0.79	7.2±1.99*	<0.001
PaO_2/FiO_2	375.71±45.12	194.80±51.23*	<0.001
BALF IL-1β (pg/ml)	10.85±3.18	99.86±32.95*	<0.001
BALF IL-18 (pg/ml)	4.86±4.08	133.07±48.47*	<0.001

Abbreviation: APACHE, acute physiology and chronic health evaluation; SOFA, sequential (sepsis-related) organ failure assessment, PaO_2/FiO_2, arterial oxygen partial pressure/fraction of inspired oxygen; BALF, bronchoalveolar lavage fluid.

*$p<0.001$.